

# The strangeness magnetic moment of the nucleon from FLIC fermions

D. B. Leinweber<sup>a</sup>, S. Boinepalli<sup>a</sup>, A. W. Thomas<sup>a</sup>, A. G. Williams<sup>a</sup>, R. D. Young<sup>a</sup>, J. M. Zanotti<sup>a,b</sup> and J. B. Zhang<sup>a</sup>

<sup>a</sup>Special Research Center for the Subatomic Structure of Matter, and  
Department of Physics, University of Adelaide Adelaide SA 5005 Australia

<sup>b</sup>John von Neumann-Institut für Computing NIC,  
Deutsches Elektronen-Synchrotron DESY, D-15738 Zeuthen, Germany

By imposing the constraints of charge symmetry we show that the strangeness magnetic moment of the nucleon can be expressed in terms of empirical magnetic moments and ratios of valence quark magnetic moments. The latter are determined using modern chiral extrapolation techniques and recent low mass lattice QCD simulations of the individual quark contributions to the magnetic moments of the nucleon octet. The result is a precise determination of  $G_M^s$ , namely  $-0.043 \pm 0.026 \mu_N$ , which is consistent with the latest experimental measurements.

## 1. INTRODUCTION

There is currently enormous interest in the determination of the strangeness content of the nucleon. It is clearly crucial to our understanding of QCD to determine precisely the role played by heavier, non-valence flavors. On the experimental side there have been tremendous advances in the ability to measure parity violation in electron scattering at the level of  $10^{-7}$  and new results on strangeness in the nucleon have been reported recently from JLab (HAPPEX) [1] and MIT-Bates (SAMPLE) [2]. In the near future we can expect even more precise results from the A4 experiment at Mainz as well as G0 and HAPPEX2 at JLab.

In contrast, the theoretical situation is somewhat confused with the predictions of various quark models covering an enormous range. Direct calculations within lattice QCD have not yet clarified the situation, with values for  $G_M^s$  ranging from  $-0.28 \pm 0.10$  [3] to  $+0.05 \pm 0.06$  [4]. We take a different approach, building on the improvements in both lattice actions and computer speed which have enabled quenched QCD (QQCD) simulations of magnetic moments at pion masses as low as 0.3–0.4 GeV and on the developments of modern chiral extrapolation techniques which allow one to rigorously ensure the model independent constraints of chiral symmetry. Using these

techniques we determine the ratios of the  $u$ -quark contribution to the magnetic moment of the physical proton to that in the  $\Sigma^+$  and of the  $u$  quark in the physical neutron to that in the  $\Xi^0$ . From these ratios, experimental data on the octet moments and charge symmetry, which is typically satisfied at the level of 1% or better [5], we deduce a new theoretical value for  $G_M^s$  which is extremely precise – setting a tremendous challenge for the next generation of parity violation experiments.

## 2. CHARGE SYMMETRY

An examination of the symmetries manifest in the QCD path integral for current matrix elements reveals various relationships among the quark contributions [6]. The magnetic moment of the proton, is extracted from the three-point function, where an operator exciting the proton from the QCD vacuum is followed by the electromagnetic current, which in turn is followed by an operator annihilating the proton back to the QCD vacuum. In calculating this three point function, one encounters two topologically distinct ways of performing the electromagnetic current insertion. Figure 1 displays skeleton diagrams for these two possible insertions (with Euclidean time increasing to the right). In full QCD these diagrams incorporate an arbitrary number of gluons

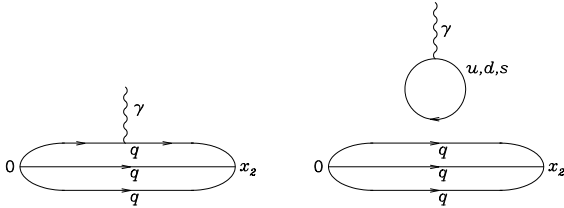


Figure 1. Diagrams illustrating the two topologically different insertions of the current within the framework of lattice QCD. These skeleton diagrams for the connected (left) and disconnected (right) current insertions may be dressed by an arbitrary number of gluons and quark loops.

and quark loops. The left-hand diagram illustrates the connected insertion of the current to one of the “valence” quarks of the baryon. In the right-hand diagram the external field produces a  $q\bar{q}$  pair which in turn interacts with the valence quarks of the baryon via gluons. It is important to realize that within the lattice QCD calculation of the loop diagram on the right side of Fig. 1 there is no anti-symmetrization (Pauli blocking) of the quark in the loop with the valence quarks. For this reason, in general only the sum of the two processes in Fig. 1 is physical.

Under the assumption of charge symmetry, the three-point correlation functions for octet baryons leads to the following equalities for electromagnetic current matrix elements [6]:

$$\begin{aligned}
 p &= e_u u^p + e_d d^p + O_N, \\
 n &= e_d u^p + e_u d^p + O_N, \\
 \Sigma^+ &= e_u u^\Sigma + e_s s^\Sigma + O_\Sigma, \\
 \Sigma^- &= e_d u^\Sigma + e_s s^\Sigma + O_\Sigma, \\
 \Xi^0 &= e_s s^\Xi + e_u u^\Xi + O_\Xi, \\
 \Xi^- &= e_s s^\Xi + e_d u^\Xi + O_\Xi.
 \end{aligned} \tag{1}$$

Here, all quantities refer to magnetic moments, so for example  $p$  and  $\Xi^-$  are the physical magnetic moments of the proton and  $\Xi^-$ , respectively. The valence  $u$ -quark magnetic moment in the proton, corresponding to the left-hand side of Fig. 1, is denoted  $u^p$ . We emphasize that charge symmetry has been used to replace the  $d$ -quark contribution in the neutron by  $u^p$ ,  $d$  in the  $\Sigma^-$  by  $u$  in the  $\Sigma^+$  (

$u^\Sigma$ ), and so on. Finally,  $O$  denotes the total contribution from quark-loops – i.e., the contribution shown on the right-hand side of Fig. 1. The labels on quark magnetic moments allow for the environment sensitivity implicit in the three-point function [6]. For example, the three-point function for the  $\Sigma^+$  is the same as that for the proton, except that the  $d$  is replaced by the somewhat heavier  $s$ -quark. Hence, the  $u$ -quark propagators in the  $\Sigma^+$  are multiplied by an  $s$ -quark propagator, whereas in the proton they are multiplied by a  $d$ -quark propagator. The different mass of the neighboring quark gives rise to an environment sensitivity in the  $u$ -quark contributions to observables, which means that the naive expectations of the constituent quark model  $u^p/u^\Sigma = u^n/u^\Xi = 1$  may not be satisfied [6,7,8,9,10,11,12,13]. This observation should be contrasted with the usual quark model assumption that the quark magnetic moment is an intrinsic property, independent of the quark’s environment.

In three-flavor QCD,  $O_N$  contains sea-quark-loop contributions from  $u$ ,  $d$  and  $s$  quarks. In the SU(3)-flavor limit ( $m_u = m_d = m_s$ ) the charges add to zero and hence the sum vanishes. However, the heavier strange quark mass leads to a non-zero result. By definition

$$O_N = \frac{2}{3} \ell G_M^{cu} - \frac{1}{3} \ell G_M^{cd} - \frac{1}{3} \ell G_M^{cs}, \tag{2}$$

$$= \frac{\ell G_M^s}{3} \left( \frac{1 - \ell R_d^s}{\ell R_d^s} \right), \tag{3}$$

where

$$\ell R_d^s \equiv \frac{\ell G_M^s}{\ell G_M^d}, \tag{4}$$

and the leading superscript,  $\ell$ , reminds one that the contributions are loop contributions. Note that, in deriving Eq.(3), we have set  $\ell G_M^u = \ell G_M^d$ , corresponding to  $m_u = m_d$  [6]. Earlier estimates of  $\ell R_d^s$  were based on the constituent quark model, however a more reliable approach is to estimate the loops using a finite range regulator [14,15,16]. Since the chiral coefficients for the  $d$  and  $s$  loops in the RHS of Fig. 1 are identical, the only difference comes from the mass of the  $K$  compared with that of the  $\pi$ .

With no more than a little accounting, the strange-quark loop contributions to the nucleon magnetic moment,  $G_M^s$  may be isolated from (1) and (3) in the following two phenomenologically useful forms,

$$G_M^s = \left( \frac{\ell R_d^s}{1 - \ell R_d^s} \right) \left[ 2p + n - \frac{u^p}{u^\Sigma} (\Sigma^+ - \Sigma^-) \right], \quad (5)$$

and

$$G_M^s = \left( \frac{\ell R_d^s}{1 - \ell R_d^s} \right) \left[ p + 2n - \frac{u^n}{u^\Xi} (\Xi^0 - \Xi^-) \right]. \quad (6)$$

As we have explained, under the assumption that quark magnetic moments are not environment dependent, these ratios (i.e.  $u^p/u^\Sigma$  and  $u^n/u^\Xi$ ) are taken to be unity in many quark models. Incorporating the experimentally measured baryon moments leads to:

$$G_M^s = \left( \frac{\ell R_d^s}{1 - \ell R_d^s} \right) \left[ 3.673 - \frac{u^p}{u^\Sigma} (3.618) \right], \quad (7)$$

and

$$G_M^s = \left( \frac{\ell R_d^s}{1 - \ell R_d^s} \right) \left[ -1.033 - \frac{u^n}{u^\Xi} (-0.599) \right], \quad (8)$$

where all moments are expressed in nuclear magnetons ( $\mu_N$ ). (Note that the measured magnetic moments are all known sufficiently accurately [17] that the experimental errors play no role in our subsequent analysis.) We stress that *these expressions for  $G_M^s$  are exact consequences of QCD, under the assumption of charge symmetry.* Equation (8) provides a particularly favorable case for the determination of  $G_M^s$  with minimal dependence on the valence-quark ratio.

If one considers the quark model suggestions of  $u^n/u^\Xi = 1$  and  $\ell R_d^s = 0.65$  in (8), one finds  $G_M^s = -0.81 \mu_N$ , a significant departure from the experimental preference of positive values.

Equating (7) and (8) provides a linear relationship between  $u^p/u^\Sigma$  and  $u^n/u^\Xi$  which must be satisfied within QCD. Figure 2 displays this relationship by the dashed and solid line, the latter corresponding to values for which  $G_M^s(0) > 0$  when  $\ell R_d^s$  is in the anticipated range  $0 < \ell R_d^s < 1$ . Since the line does not pass through the point (1.0, 1.0) corresponding to the simple

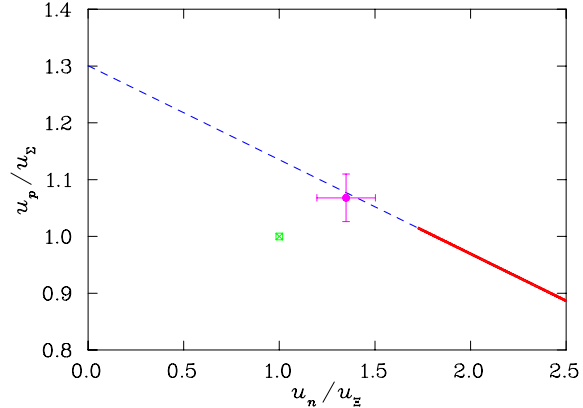


Figure 2. The consistency relation between  $u^p/u^\Sigma$  and  $u^n/u^\Xi$  which must be satisfied within QCD. The part of the straight line which is dashed corresponds to  $G_M^s(0) < 0$ , while the solid part of the line has  $G_M^s(0) > 0$ . The standard quark model assumption of intrinsic quark moments independent of their environment is indicated by the filled square. The lattice QCD prediction (after an appropriate chiral extrapolation, discussed in following sections) is illustrated by the filled circle.

quark model assumption of universality, the experimentally measured baryon moments are signaling that there must be an environment effect exceeding 12% in both ratios or approaching 20% or more in at least one of the ratios. Moreover, a positive value for  $G_M^s(0)$  requires an environment sensitivity exceeding 70% in the  $u^n/u^\Xi$  ratio. Hence the experimental suggestion that  $G_M^s(0) > 0$  challenges the intrinsic magnetic moment concept which is fundamental to the constituent quark model.

### 3. NUMERICAL SIMULATIONS WITH FLIC FERMIONS

Access to leading-edge supercomputing resources coupled with advances in the formulation of computationally-inexpensive chirally-improved lattice fermion actions enable the numerical calculation of hadron structure near the chiral regime. The numerical simulations of the

electromagnetic form factors presented here are carried out using the Fat Link Irrelevant Clover (FLIC) fermion action [18,19] in which the irrelevant operators introduced to remove fermion doublers and lattice spacing artifacts are constructed with smoothed links. These links are created via APE smearing [20]; a process that averages a link with its nearest transverse neighbors in a gauge invariant manner. Iteration of the averaging process generates a “fat” link.

The use of links in which short-distance fluctuations have been removed simplifies the determination of the coefficients of the improvement terms in both the action and its associated conserved vector current. Perturbative renormalizations are small for smeared links and the mean-field improved coefficients used here are sufficient to remove  $\mathcal{O}(a)$  errors, in the lattice spacing  $a$ , from the lattice fermion action. The key is that both the energy dimension-five Wilson and Clover terms [21] are constructed with smooth links, while the relevant operators, surviving in the continuum limit, are constructed with the original untouched links generated via standard Monte Carlo techniques.

FLIC fermions provide a new form of nonperturbative  $\mathcal{O}(a)$  improvement [19,22] where near-continuum results are obtained at finite lattice spacing. Access to the light quark mass regime is enabled by the improved chiral properties of the lattice fermion action. The magnitude of additive mass renormalizations is suppressed [22] which otherwise can lead to singular behavior in the propagators as the quarks become light.

The  $\mathcal{O}(a)$ -improved conserved vector current [23] is used. Nonperturbative improvement is achieved via the FLIC procedure where the terms of the Noether current having their origin in the irrelevant operators of the fermion action are constructed with mean-field improved APE smeared links. The preliminary results presented here are from a sample of  $255 \cdot 20^3 \times 40$  mean-field improved Luscher-Weisz [24] gauge field configurations having a lattice spacing of 0.128 fm as determined by the Sommer scale  $r_0 = 0.50$  fm.

#### 4. CHIRAL EXTRAPOLATION

One of the major challenges at present in connecting lattice calculations of hadronic properties with the physical world is that computational limitations restrict the accessible quark masses to values much larger than the physical values. At quark masses typical of today’s lattice QCD simulations, one is outside the region where traditional dimensionally regulated (DR) chiral perturbation theory ( $\chi$ PT) is applicable. Yet one knows that for current quark masses near zero there is important non-analytic structure (as a function of the quark mass) which must be treated correctly if we are to compare with physical hadron properties.

Our present analysis of the strangeness magnetic form factor has been made possible by a significant breakthrough in the regularization of the chiral loop contributions to hadron observables [14,15]. Through the process of regulating loop integrals via a finite-range regulator [14], the chiral expansion is re-summed producing an expansion with vastly improved convergence properties.

The key feature of finite-range regularization (FRR) is that FRR schemes have an additional adjustable regulator parameter which provides an opportunity to suppress short distance physics from the loop integrals of effective field theory. This short-distance physics is otherwise treated incorrectly as the naive effective fields do not share the properties of QCD at short distances.

An extensive study of the quark mass dependence of the nucleon mass in finite-range regularized (FRR)  $\chi$ PT [14] explored six different regularization and associated renormalization schemes. The smooth regulators (dipole, monopole, or Gaussian regulators) provide expansions that agree over the range  $0 \leq m_\pi^2 < \sim 0.8 \text{ GeV}^2$  at a level sufficient to predict the nucleon mass within 1%. Our focus here is to extrapolate FLIC fermion calculations of valence quark contributions to baryon moments ( $u^p$ ,  $u^n$ ,  $u^\Sigma$ ,  $u^\Xi$ ) to the physical mass regime. We select the dipole-vertex FRR with  $\Lambda = 0.8 \text{ GeV}$  as determined in Ref. [25]. This scale was found to give the best simultaneous description of both quenched and dynamical simulation results.

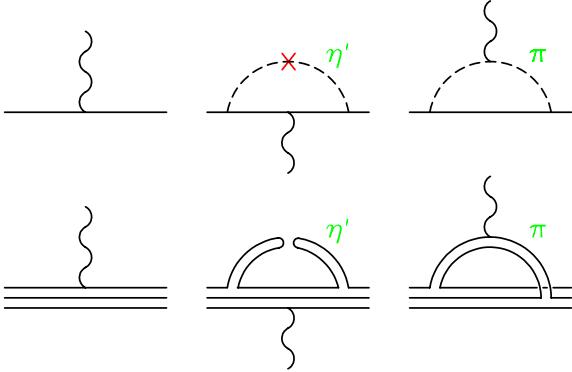


Figure 3. Diagrams providing the leading contributions to the chiral expansion of baryon magnetic moments (upper diagrams) and their associated quark flows (lower diagrams) in QQCD. In the lower diagrams, the quark-photon coupling is summed over adjacent quark lines.

Separation of the valence and sea-quark-loop contributions to the meson cloud of full QCD hadrons is a non-trivial task. We use the diagrammatic method for evaluating the quenched chiral coefficients of leading nonanalytic terms in heavy-baryon quenched  $\chi$ PT [26,27]. These results are generalized to the FRR approach used here. The diagrammatic technique provides a transparent means to accomplish the separation of magnetic moment contributions in full-QCD into “direct sea-quark loop” and “valence” contributions as in the discussion surrounding Fig. 1. The valence contributions (key to this analysis) are obtained by removing the direct-current coupling to sea-quark loops from the total contributions. Upon further removing “indirect sea-quark loop” contributions, where a valence quark forms a meson composed with a sea-quark loop, one obtains the “quenched valence” contributions, the conventional view of the quenched approximation. Isolating a particular quark flavour contribution only requires setting the electric charge of all other quark flavours to zero.

Figure 3 displays the diagrams providing the leading contributions to the chiral expansion of baryon magnetic moments (upper diagrams) and their associated quark flows in quenched QCD

(QQCD). The associated chiral expansion for the proton magnetic moment,  $\mu_p$ , has the form

$$\mu_p = a_0^\Lambda + \mu_p \chi_{\eta'} I_{\eta'}(m_\pi, \Lambda) + \chi_\pi I_\pi(m_\pi, \Lambda) + \chi_K I_K(m_K, \Lambda) + a_2^\Lambda m_\pi^2 + a_4^\Lambda m_\pi^4. \quad (9)$$

where  $I$  denotes a loop integral defined by

$$I_\pi(m_\pi, \Lambda) = -\frac{4}{3\pi} \int_0^\infty dk \frac{k^4}{(k^2 + m_\pi^2)^2} u^2(k, \Lambda) \quad (10)$$

$$I_K(m_K, \Lambda) = -\frac{4}{3\pi} \int dk \frac{k^4 u^2(k)}{(k^2 + m_K^2)(\sqrt{k^2 + m_K^2} + \Delta_{BN})^2} \quad (11)$$

$$I_{\eta'}(m_\pi, \Lambda) = -\int_0^\infty dk \frac{k^4}{(k^2 + m_\pi^2)^{\frac{5}{2}}} u^2(k, \Lambda) \quad (12)$$

where  $\Delta_{BN}$  is the physical mass-splitting between the  $N$  and  $\Sigma$  or  $\Lambda$ . The coefficients,  $\chi$ , denote the model-independent coefficients of the LNA term for  $\pi$  and  $K$  mesons [27]. We take

$$m_K^2 = m_K^{(0)2} + \frac{1}{2} m_\pi^2 \quad (13)$$

where the physical values may be used to define  $m_K^{(0)}$ . The  $m_\pi^4$  term of Eq. (9) allows for some curvature associated with the Dirac moment of the baryon  $\propto 1/m_\pi^2$  for moderately large quark masses.

The un-renormalized coefficients of the analytic terms of the FRR expansion are regulator-parameter dependent. This is emphasized by the superscript  $\Lambda$  on the coefficients  $a_0$ ,  $a_2$  and  $a_4$ . The large  $m_\pi$  behavior of the loop integrals of Eq. (9) and the residual expansion are remarkably different. Whereas the residual expansion will encounter a power divergence, the FRR loop integrals will tend to zero as some power of  $\Lambda/m_\pi$ , as  $m_\pi$  becomes large. Thus, the  $\Lambda$  dependence of  $a_0$ ,  $a_2$  and  $a_4$  provides an opportunity to govern the convergence properties of the residual expansion and thus the FRR chiral expansion.

Lattice QCD has now provided extensive model-independent information on the moderate to large  $m_\pi$  dependence of hadron observables. In particular, hadron masses are observed to be smooth almost linear functions of  $m_\pi^2$  for quark masses similar to the strange quark mass. The magnetic moments presented here are also smooth, taking on a Dirac moment dependence

as the quark mass becomes large. This indicates that it should be possible to tune the regulator-range parameter,  $\Lambda$ , such that the coefficients  $a_4$ , and higher are truly small. In this case the convergence properties of the residual expansion, and the loop expansion are excellent and their truncation benign. Indeed this hypothesis was confirmed for the nucleon mass in Ref. [14].

It is important to note that the optimal  $\Lambda$  is one that optimizes the convergence properties of the residual expansion. A poor choice for  $\Lambda$  will move strength in terms proportional to  $1, m_\pi^2, m_\pi^4, \dots$  from the loop integrals into the residual expansion, changing the convergence properties of the FRR expansion. We emphasize that the optimal  $\Lambda$  is *not* selected to approximate the higher-order terms of the chiral expansion. If an infinite number of parameters were being approximated by one, one would have an uncontrolled error. Fortunately such ambitions are not necessary. The lattice QCD results indicate that these higher order terms of the chiral expansion largely sum to zero. Moreover, the findings of Ref. [14] indicate that the details of exactly how each of the terms enters the vanishing sum are largely irrelevant.

Perhaps it is also worth emphasizing that the choice of  $\Lambda$  can have no effect on the convergence properties of the renormalized chiral expansion. There, contributions from the residual expansion and the FRR loop integrals are combined, removing any  $\Lambda$  dependence from the chiral expansion. This is the process of renormalization.

Donoghue *et al.* [28] describe the convergence problems of DR as due to incorrect short-distance physics in loop integrals which must be removed by large and opposing analytic-term contributions. The introduction of an ultraviolet cut off in FRR schemes prevents the error from being made in the first place and provides the opportunity to have excellent convergence properties in the residual expansion. In other words, the higher-order analytic terms of the FRR residual expansion do not need to be large, as incorrect short distance physics has been suppressed from the loop integrals. The beauty of the FRR procedure is that upon renormalization, very large coefficients can be recovered [15].

Figure 4 illustrates a fit of FRR Q $\chi$ PT to the

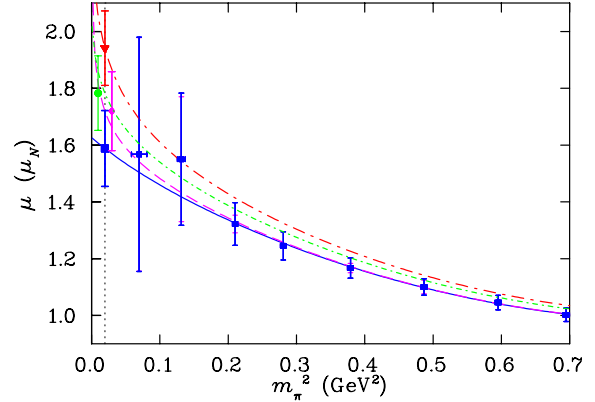


Figure 4. The contribution of a single  $u$  quark normalized to unit charge to the magnetic moment of the proton. Lattice simulation results (square symbols for  $m_\pi^2 > 0.05$  GeV) are extrapolated to the physical point (vertical dashed line) in finite-volume QQCD with a discrete momentum sum (solid curve, square symbol), and in infinite-volume QQCD (long-dashed curve, diamond symbol). Estimates of the valence  $u$  quark contribution in full QCD (dot-dash curve, triangular symbol) and the full  $u$  quark sector contribution in full QCD (fine-dash curve, circular symbol) normalized to a single quark unit charge are also illustrated. Extrapolated values indicated by symbols at the physical pion mass (vertical dashed line) are offset for clarity.

FLIC fermion lattice results (solid curve), in a calculation where only the discrete momenta allowed in the finite volume of the lattice are summed in performing the loop integral. The long-dashed curve that also runs through the lattice results illustrates the case when the discrete momentum sum is replaced by the infinite-volume, continuous momentum integral. For all but the lightest quark mass, finite volume effects are negligible.

The coefficients of the residual expansion,  $a_0^\Lambda$ ,  $a_2^\Lambda$ ,  $a_4^\Lambda$ , show excellent signs of convergence with values 1.52(14),  $-1.23(48)$ , and 0.69(42) in appropriate powers of GeV, respectively.

Incorporating baryon mass splittings into the kaon loop contributions is essential. For example the contribution of  $\Sigma \rightarrow NK$  is nearly doubled

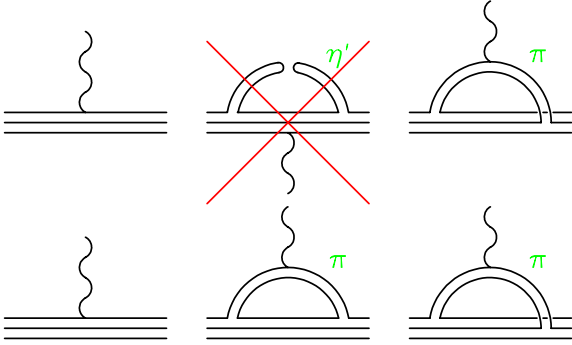


Figure 5. Correcting Q $\chi$ PT (upper diagrams) to full QCD (lower diagrams). Quenched negative-metric  $\eta'$  contributions must be removed, while the chiral coefficients of  $\pi$  and  $K$  loops must be adjusted to account for the new diagram where a valence quark couples to the photon in a meson constructed from a sea-quark loop. Photon couplings to the anti-quark in the bottom-right diagram are also included in the valence quark contributions to the nucleon moment of full QCD.

when the  $\Sigma - N$  mass splitting is taken into account.

Figure 5 diagrammatically illustrates the considerations in correcting the quenched  $u$ -quark contribution to the valence  $u$ -quark contribution in full QCD. The removal of quenched  $\eta'$  contributions and the appropriate adjustment of  $\pi$  and  $K$  loop coefficients as detailed in Ref. [26,27] provides the dot-dash curve of Fig. 4. This is our best estimate of the valence  $u$ -quark contribution (the connected insertion of the current) to the proton magnetic moment of full QCD. The graph corresponds to a single  $u$ -quark contribution normalized to unit charge. It will be interesting to confront this curve with full QCD simulation results in the future.

Finally we also include the disconnected insertion of the current in order to estimate the total contribution of the  $u$ -quark sector to the proton magnetic moment. This is represented by the fine dashed curve in Fig. 4 where the sector contribution is normalized to a single quark of unit charge. Figures 6, 7 and 8 display similar results for the  $\Sigma^+$ ,  $n$  and  $\Xi^0$ .

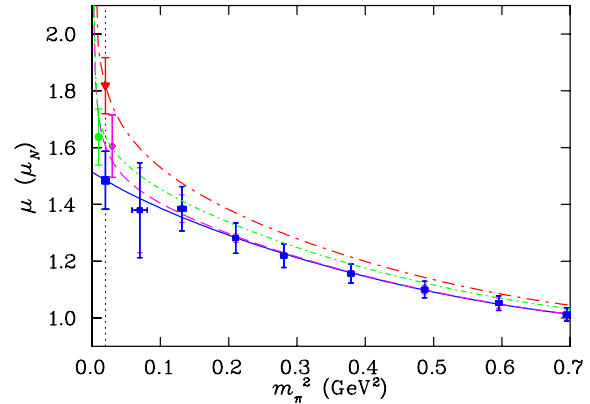


Figure 6. The contribution of a single  $u$  quark normalized to unit charge to the magnetic moment of  $\Sigma^+$ . Curves and symbols are as described in Fig. 4.

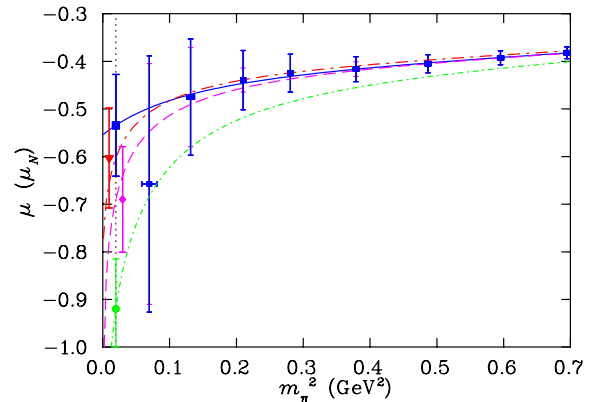


Figure 7. The contribution of the  $u$  quark normalized to unit charge to the magnetic moment of the neutron. Curves and symbols are as described in Fig. 4.

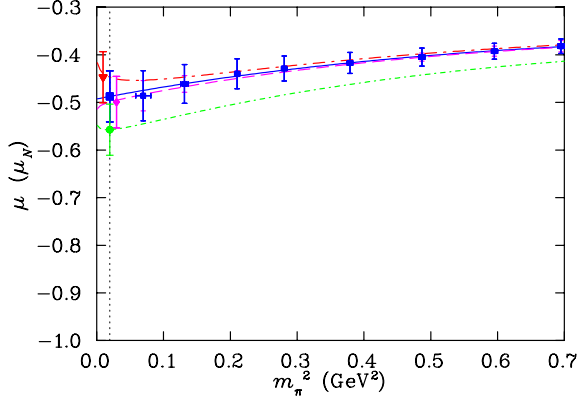


Figure 8. The contribution of the  $u$  quark normalized to unit charge to the magnetic moment of  $\Xi^0$ . Curves and symbols are as described in Fig. 4.

From these chiral extrapolations, we estimate the ratio of the valence (connected)  $u$ -quark contribution to the proton to that in  $\Sigma^+$ . Similarly, the ratio of the  $u$ -quark contribution to the neutron relative to that in  $\Xi^0$  is calculated. Error bars are estimated from a third-order single-elimination jackknife analysis of the correlated ratios. Our final result of

$$\frac{u^p}{u^\Sigma} = 1.07 \pm 0.04 \quad \text{and} \quad \frac{u^n}{u^\Xi} = 1.35 \pm 0.15 \quad (14)$$

is plotted in Fig. 2. This result leaves little doubt that  $G_M^s$  is negative. The fact that this point lies exactly on the constraint curve is highly nontrivial, and provides a robust check on the validity of the analysis techniques presented here.

As a further check we compare the lattice QCD predictions of the baryon magnetic moments constructed from extrapolations of the individual quark sectors in Fig. 9. The results display an unprecedented agreement with experiment. There is a hint of a small systematic error that suppresses the singly represented quark contribution to both  $\Xi$  baryons and the neutron. We have identified contributions from decuplet baryons as key to resolving this minor discrepancy. However, the ratio of  $u^n/u^\Xi$  does not appear to be affected by this contribution, as evidenced by the excellent agreement between lattice and experiment

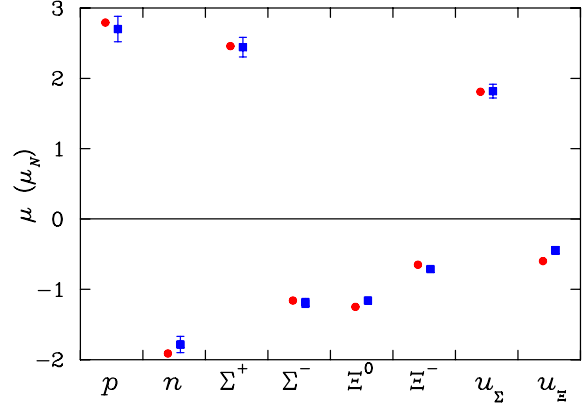


Figure 9. Comparison of the FRR $\chi$ PT extrapolated lattice QCD simulation results (square symbols) with experimentally measured baryon magnetic moments (circular symbols).

for the  $u$  quark in  $\Sigma$  and the degree of consistency between the lattice extrapolations and the constraint curve of Fig. 2. The fact that systematic errors will cancel in taking the ratios of specific quark contributions was the main motivation for introducing the ratios in the first place.

While  $G_M^s$  is most certainly negative, it remains to set the magnitude. This requires an estimate of the strange to light sea-quark loop contributions,  ${}^\ell R_d^s$ . Earlier estimates of  ${}^\ell R_d^s$  were based on the constituent quark model, however a more reliable approach is to estimate the loops using a finite range regulator [14,15]. Using a dipole-vertex regulator, a direct calculation provides

$${}^\ell R_d^s = \frac{G_M^s}{G_M^d} = 0.160 \pm 0.060, \quad (15)$$

where the range includes the variation of the dipole mass parameter between 0.6 and 1.0 GeV as well as the possible variation of the mass of the strange baryon accompanying the  $K^+$  loop. Using this value in Eq. (6) with the results of Eq. (14) provides the final precise determination of

$$G_M^s = -0.043 \pm 0.026 \mu_N, \quad (16)$$

for the strange quark contribution to the magnetic moment of the nucleon. This extremely pre-



cise value sets a tremendous challenge for the next generation of parity violation experiments.

### Acknowledgments

We thank the Australian Partnership for Advanced Computing (APAC) for generous grants of supercomputer time which have enabled this project. This work is supported by the Australian Research Council.

### REFERENCES

1. K. A. Aniol *et al.* [HAPPEX Collaboration], Phys. Lett. B **509**, 211 (2001) [arXiv:nucl-ex/0006002].
2. R. Hasty *et al.* [SAMPLE Collaboration], Science **290**, 2117 (2000) [arXiv:nucl-ex/0102001].
3. N. Mathur and S. J. Dong [Kentucky Field Theory Collaboration], Nucl. Phys. Proc. Suppl. **94** (2001) 311 [arXiv:hep-lat/0011015].
4. R. Lewis, W. Wilcox and R. M. Woloshyn, Phys. Rev. D **67** (2003) 013003 [arXiv:hep-ph/0210064].
5. G.A. Miller, B.M. Nefkens and I. Slaus, Phys. Rept. **194** (1990) 1.
6. D.B. Leinweber, Phys. Rev. **D53**, 5115 (1996) hep-ph/9512319.
7. T. D. Cohen and D. B. Leinweber. Comments Nucl. Part. Phys. **21**, 137 (1993) hep-ph/9212225; A.W. Thomas, Austral. J. Phys. **44**, 173 (1991).
8. D. B. Leinweber, R. M. Woloshyn, and T. Draper, Phys. Rev. **D43**, 1659 (1991).
9. D. B. Leinweber, Phys. Rev. **D45**, 252 (1992).
10. D. B. Leinweber, T. Draper, and R. M. Woloshyn. Phys. Rev. **D46**, 3067 (1992) hep-lat/9208025.
11. D. B. Leinweber, Phys. Rev. **D47**, 5096 (1993) hep-ph/9302266.
12. D. B. Leinweber, A. W. Thomas and R. D. Young, Phys. Rev. Lett. **86**, 5011 (2001) [arXiv:hep-ph/0101211].
13. D. B. Leinweber and A. W. Thomas, Phys. Rev. D **62** (2000) 074505 [arXiv:hep-lat/9912052].
14. R. D. Young *et al.*, Prog. Part. Nucl. Phys. **50** (2003) 399 [arXiv:hep-lat/0212031].
15. D. B. Leinweber, A. W. Thomas and R. D. Young, arXiv:hep-lat/0302020.
16. I. C. Cloet, D. B. Leinweber and A. W. Thomas, Phys. Lett. B **563** (2003) 157 [arXiv:hep-lat/0302008].
17. Particle Data Group, Phys. Rev. **D66** (2002) 010001.
18. J. M. Zanotti *et al.* [CSSM Lattice Collaboration], Phys. Rev. D **65** (2002) 074507 [arXiv:hep-lat/0110216].
19. D. B. Leinweber *et al.*, arXiv:nucl-th/0211014.
20. M. Falcioni *et al.*, Nucl. Phys. **B251**, 624 (1985).
21. S. O. Bilson-Thompson *et al.*, Annals Phys. **304** (2003) 1 [arXiv:hep-lat/0203008].
22. J. Zanotti, *et al.*, in preparation.
23. G. Martinelli, C. T. Sachrajda and A. Vladikas, Nucl. Phys. B **358** (1991) 212.
24. M. Luscher and P. Weisz, Commun. Math. Phys. **97**, 59 (1985) [ibid. **98**, 433 (1985)].
25. R. D. Young, D. B. Leinweber, A. W. Thomas and S. V. Wright, Phys. Rev. D **66**, 094507 (2002) [arXiv:hep-lat/0205017].
26. D. B. Leinweber, Nucl. Phys. Proc. Suppl. **109A** (2002) 45 [arXiv:hep-lat/0112021].
27. D. B. Leinweber, arXiv:hep-lat/0211017.
28. J. F. Donoghue, B. R. Holstein and B. Borasoy, Phys. Rev. **D59**, 036002 (1999).